Production of Carbon Nanofibers in High Yields Using a Sodium Chloride Support

Junfeng Geng,[†] Ian A. Kinloch,[‡] Charanjeet Singh,[‡,§] Vladimir B. Golovko,[†] Brian F. G. Johnson,*[,†] Milo S. P. Shaffer,[‡,||] Yali Li,[‡] and Alan H. Windle[‡]

Department of Chemistry, Cambridge University, Cambridge CB2 1EW, United Kingdom, and Department of Materials Science and Metallurgy, Cambridge University, Cambridge CB2 3QZ, United Kingdom

Received: March 25, 2005; In Final Form: April 13, 2005

A new route for the highly convenient scalable production of carbon nanofibers on a sodium chloride support has been developed. Since the support is nontoxic and soluble in water, it can be easily removed without damage to the nanofibers and the environment. Nanofiber yields of up to 6500 wt % relative to the nickel catalyst have been achieved in a growth time of 15 min. Electron microscopy (SEM, TEM) and thermal gravimetric analysis (TGA) indicated that the catalytically grown carbon had relatively little thermal overgrowth and possessed either a herringbone or a semi-ordered nanostructure, depending on the growth conditions.

1. Introduction

Carbon nanotubes and nanofibers show promise in a range of industrial applications due to their unique combination of mechanical, electrical, thermal, and chemical properties.[1−4] Among the many synthetic routes for these nanostructures, the chemical vapor deposition (CVD) route is mainly favored because of its scalability and potentially low cost.[5−8] In CVD, the catalytic metal nanoparticles are often coated onto a solid support to prevent sintering at high growth temperatures (600 to 1000 °C). Widely employed supports include silica (SiO_2), alumina (Al_2O_3), titania (TiO_2) or magnesium oxide (MgO) because of their chemical inertness and high-temperature resistance.[5−12] However, all of these refractory materials require highly concentrated bases (e.g., NaOH) or strong acids (e.g., HF) to remove them, and these reagents may also damage the carbon nanostructure. Additionally, strong acids and bases are less desirable for large-scale production due to environmental concerns.

The use of a water-soluble catalyst support would provide a natural solution to these problems but has not been much studied, despite the large body of literature on CVD syntheses. To the best of our knowledge, there is only one report about the growth of carbon nanofibers on a water-soluble substrate. In their paper, Szabo et al.,[13] used cobalt nitrate ($Co(NO_3)_2 \cdot 6H_2O$) as the catalytic precursor and sodium chloride (NaCl) powder as the support. However, the reported synthesis is not satisfactory because of the low carbon yield (2.6 wt % relative to the weight of support), the volume of side-products (mainly carbon-encapsulated Co nanoparticles), and the presence of amorphous carbon (indicated by significant weight-loss at a temperature around 300 °C, in the thermal gravimetric analysis). In fact, earlier literature suggested that it was not possible to grow one-dimensional carbon nanostructures, such as nanotubes or nanofibers, on sodium chloride substrate.[14] Here we report a new approach to the synthesis of carbon nanofibers (CNFs) using a NaCl support. A range of catalyst precursors has been investigated under different reaction conditions. In particular, nickel stearate has been found to be an efficient precursor for coating the salt support, and the resultant catalyst had led to the production of CNFs in both high purity and yields, without forming carbon-encapsulated metal nanoparticles.

2. Experimental Section

The catalyst precursors were coated onto the salt substrate by two different methods, depending on the solubility of the precursor in organic solvents. In both cases, the relative loading of the metal was kept low to minimize sintering. In the first method, the catalyst precursor was dissolved in a solvent in which the NaCl support was insoluble. For example, nickel stearate (fine waxy powder, $(CH_3(CH_2)_{16}COO)_2Ni$, Strem Chemical Ltd.) was coated onto a sodium chloride powder (Sigma Aldrich) by dissolving the stearate in toluene, in which the NaCl was then suspended. A typical catalyst preparation involved fully dissolving 532 mg of nickel stearate into 30 mL of freshly distilled toluene. Next, 10 g of sodium chloride was added, and the mixture was vigorously stirred for 20 min so that the salt powder was fully suspended in the solution. The temperature of the liquid was kept at 95 °C. The toluene was removed under a reduced pressure, during which process the stearate gradually precipitated from the solution and coated onto the salt grains as a thin film. The resultant catalyst/support was dried at 100 °C.

The second method, using two solvents, was used to prepare the nickel formate/NaCl and iron acetate/NaCl catalysts. Here, the catalyst precursors were first dissolved in methanol, and the resultant methanol solution was then slowly added to a toluene suspension of the chloride support under vigorous stirring and at a temperature above the boiling point of methanol but lower than that of toluene. Following the rapid removal of methanol under a reduced pressure, the precursors precipitated from the solution and deposited on the surface of the salt powder. In this way, the precursor/support catalysts with a variety of metal loadings were prepared. For example, a formate/NaCl catalyst was prepared by suspending 10 g of NaCl powder in 50 mL of toluene. To this was addded dropwise 10 mL of

* To whom correspondence should be addressed. E-mail: bfgj1@cam.ac.uk. Tel: +44 1223 336337. Fax: +44 1223 336017.
† Department of Chemistry, Cambridge University.
‡ Department of Materials Science and Metallurgy, Cambridge University.
§ Present address: Thomas Swan Co. & Ltd., Consett, County Durham, DH8 7ND United Kingdom.
|| Present address: Department of Chemistry, Imperial College, London, SW7 2AZ United Kingdom.

10.1021/jp051544w CCC: $30.25
Published on Web 08/12/2005

TABLE 1: Summary of the Catalysts Used, Metal Loadings, CVD Parameters, Yields, and Carbon Nanostructures of the Produced Carbon Nanofibers

catalytic precursor (on the salt support)	metal loading and gas flow rate (mL/min)	yield 1 (relative to the mass of salt support) wt %	yield 2 (relative to the mass of pure metal) wt %	carbon growth rate g(C)/g(M)/min	morphology of the CNFs
nickel stearate	0.5 wt % Ni, 620 °C, $C_2H_2 = 130$, Ar = 1300	32.7	6534	4.4	straight, long NFs with diameters of 30−80 nm, hollow and a semi- ordered crystalline structure within the walls; D/G ratio of 1 in Raman
nickel formate	0.16 wt % Ni, 650 °C, $C_2H_2 = 20$, Ar = 200	7.7	5241	1.8	highly curved NFs with diameters of 20−60 nm and a herringbone structure within the walls. D/G ratio of 2 in Raman
iron acetate	0.03 wt % Fe, 650 °C, $C_2H_2 = 20$, Ar = 200	2.3	7919	2.6	curved NFs with diameters of 20−60 nm; poorly ordered graphitic walls; D/G ratio of 1 in Raman.

methanol solution of nickel formate (concentration in Ni: 5.4×10^{-3} M). While the mixture was vigorously stirred, the methanol was removed at 80 °C under a reduced pressure. The toluene was finally removed at 100 °C, and the resultant sample was dried at ~90 °C overnight.

For growth of CNFs using the CVD technique, the as-prepared catalyst/NaCl powder was ground and loaded into an alumina boat. The boat was introduced into a preheated reaction tube containing an argon atmosphere, causing thermolysis of the catalyst precursor and formation of the metallic nanoparticles. On introduction of the reaction gas (acetylene), the growth of carbon nanofibers occurred. Initially, scouting experiments were carried out to assess the growth conditions. Detailed studies were then conducted on the most promising conditions identified.

The products were examined by scanning transmission electron microscopy (SEM, JEOL 6340 at 5 kV) and transmission electron microscopy (TEM, JEOL JEM-3010x at 300 kV). The Raman spectroscopic studies were performed by a Renishaw 1000 micro-Raman spectrometer using an excitation Ar^+ laser at $\lambda = 514.5$ nm. Thermal gravimetric analysis (TGA) was conducted on the reacted catalysts using an air atmosphere in order to obtain both the yield and the type of carbon produced (Perkin-Elmer TGA7, 10 °C/min). These samples were ground before the analysis in order to prevent cracking of the NaCl support which led to physical loss of the sample from the measuring pan. TGA was also conducted on the catalyst precursors to understand their decomposition pathways (Thermal Analysis Q500, nitrogen atmosphere, dynamic heating).

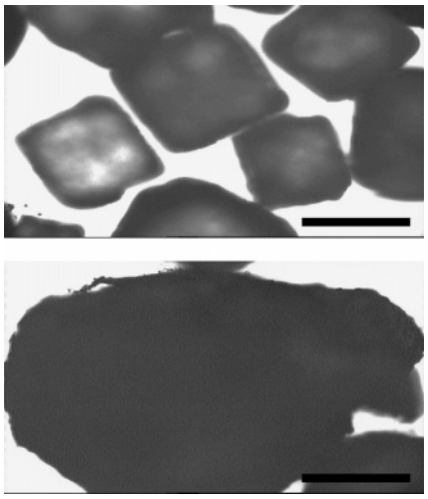

Figure 1. Optical microscopic images showing the NaCl grains before and after the growth of CNFs. Upper image: before the growth, the grains with a coated thin layer of nickel stearate. Lower image: a typical salt grain after the growth. This image shows a dramatic increase of the volume due to abundant CNFs covered on the salt surface. Scale bar: 500 μm.

3. Results and Discussion

3.1. Scouting Experiments. The melting point of NaCl is 820 °C; however, its partial pressure is significant even at lower temperatures. A noticeable salt deposit was observed in the cold end of the reaction tube at temperatures as low as 760 °C. Therefore, all of the experiments conducted were at a maximum temperature of 760 °C in an attempt to minimize NaCl surface disruption. Two carbon feedstocks were used for the scouting experiments, methane and acetylene. The latter was thermodynamically least stable and hence most suitable for the low-temperature reactions.

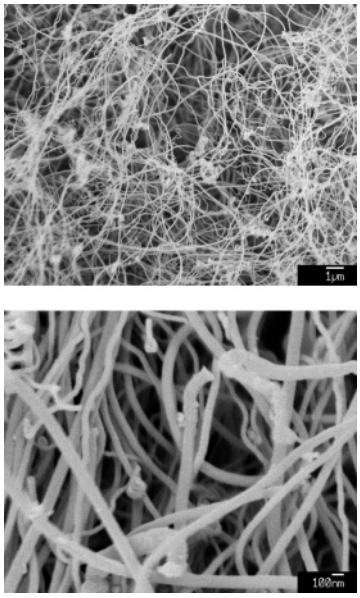

Figure 2. SEM images of the CNFs grown on the nickel stearate/NaCl catalyst. Both images were from the same sample but at different magnifications to show the abundance and cleanness of the product. The CVD growth was performed using C_2H_2 as the carbon feedstock at 620 °C, with a ratio of C_2H_2: Ar = 1: 10, and the flow rate of Ar at 1.3 l min^{-1}.

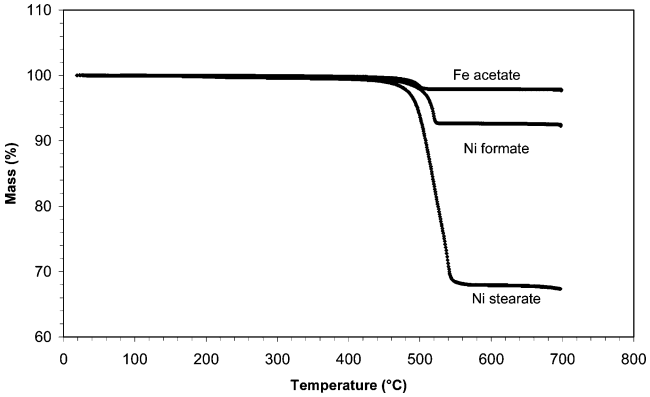

Figure 3. TGA analysis of the yields of the CNFs produced by three different catalytic precursors: nickel stearate, nickel formate and iron acetate. Samples were heated in air, with a temperature increasing rate of 10 °C/min.

A variety of experiments were conducted with methane−argon mixture using various volume ratios (1:0, 1:1, 1:2, and 1:3) at reaction temperatures between 650 and 760 °C. In general, no carbon deposition occurred on the stearate-coated salt surface. For the nickel formate catalyst, only small particles (20−200 nm in diameter) were observed beneath 700 °C, whereas at higher temperatures, a very few nanofibers were also present. These results were unexpected since the growth conditions were known to lead successful nanotube growth when using a fumed silica substrate rather than NaCl. The exact sintering process of the metal nanoparticles on the NaCl is not yet known, but it is probably affected by the initially smooth surface of the NaCl and evaporation at higher temperatures. SEM observation revealed that the surface of the sodium chloride powder changed significantly after heating at 760 °C, with cracks and layers being observed. Partial melting also occurred at the defect or corner locations of the salt crystals.

Acetylene reactions were found to be more successful than the methane ones, with nanofibers produced at 650 °C from all the three types of NaCl-supported catalysts. The acetylene was diluted with argon with a ratio of typically 1:10 (C_2H_2:Ar). The optimal reaction conditions identified (Table 1) are discussed in more detail in sections 3.2 and 3.3.

3.2. Production of Carbon Nanofibers from the Stearate/NaCl Catalyst. The optical micrographs, Figure 1, show the morphologies of the sodium chloride powder before and after the nanofiber growth. The effective volume of each salt grain was found to greatly increase due to the coverage by the CNFs, as confirmed by the SEM analysis (Figure 2). These CNFs were straight, typically ∼30 μm long, possessed a clean surface, and had an outer diameter of 20−80 nm. In a post-growth treatment, putting the CNFs product into hot water led to a noticeable dissolution and thus removal of the NaCl support.

Thermo-gravimetric analysis of the product showed that no weight loss occurred in air until 440 °C, with the main loss at 490 °C (Figure 3). Comparing this with the burning temperature of ∼300 °C for amorphous carbon[2,15] and ∼600 °C for CVD grown multiwall nanotubes, we suggest that the produced CNFs contained relatively little amorphous carbon although they did have defects and/or exposed graphitic edges. The carbon yield, in a growth time of 15 min, was 32.7 wt % relative to the total mass of the support and catalyst and 6534 wt % relative to the

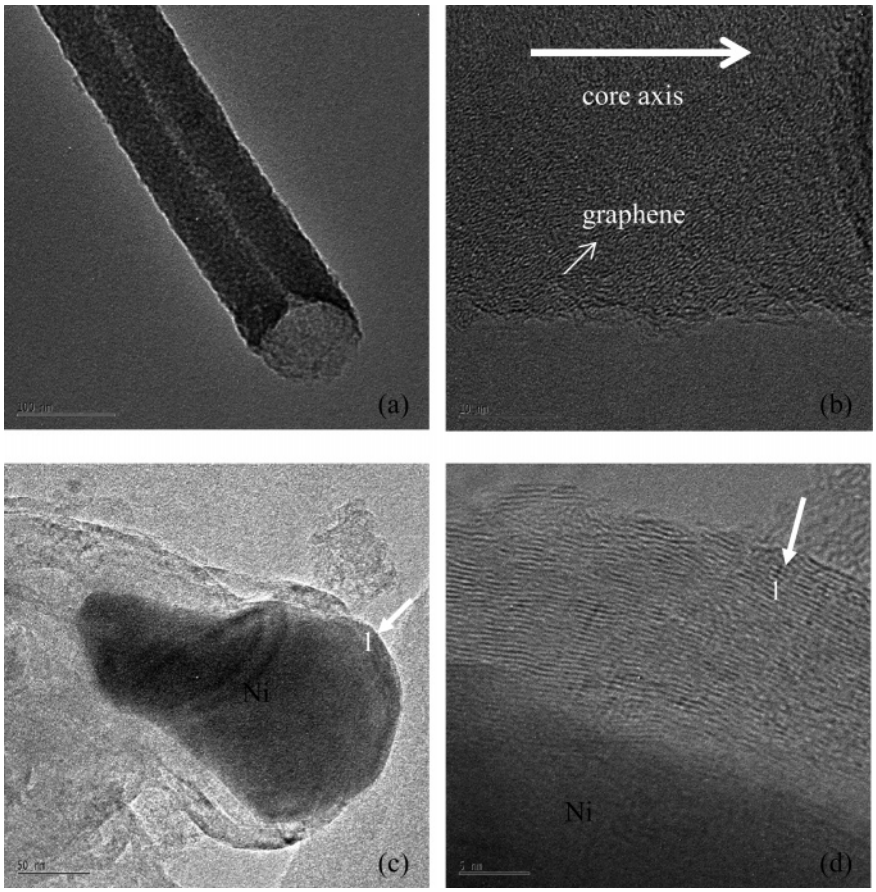

Figure 4. Set of TEM images of the CNFs produced using the nickel stearate/sodium chloride catalyst. (a) A typical nanofiber with an open end; (b) An image showing the typical structure of the fiber wall; (c) Image at a fiber-tip position showing the metal nanoparticle and its surrounding carbon; (d) Detailed structure of the carbon surrounding the metal particle, as indicated by arrow 1. This image shows the well crystalline graphite fringes.

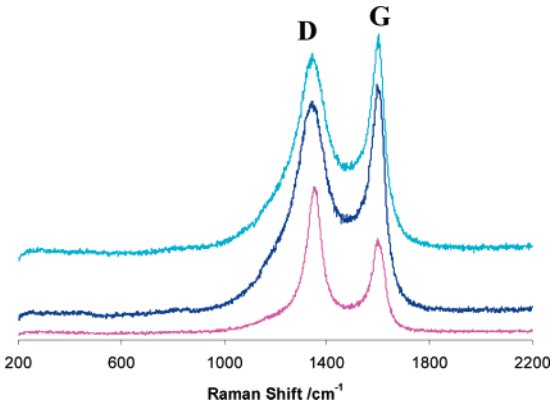

Figure 5. Raman spectra of the as-prepared CNFs using different catalysts on a sodium chloride support. Top curve corresponds to nickel stearate/support catalyst. Middle curve corresponds to iron acetate/support catalyst. Bottom curve corresponds to nickel formate/support catalyst. All three profiles show both the G and D peak. The CNFs were grown in CVD using C_2H_2 as the carbon feedstock at 620−650 °C. The excitation wavelength of the laser for this measurement was 514 nm.

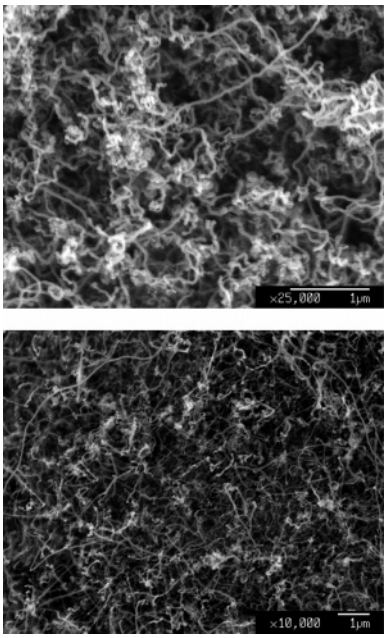

Figure 6. SEM images of CNFs produced by using nickel formate or iron acetate as the catalyst precursor on a sodium chloride support. Top image: the as-prepared CNFs on the formate/NaCl powder. In this case, the metal loading in pure Ni was 0.16 wt %, relative to the mass of the salt support. Bottom image: the as-prepared CNFs on the acetate/NaCl powder. The metal loading in pure Fe was 0.03 wt %, relative to the mass of the salt support. CVD growth was performed by using C_2H_2 as the carbon source, at 650 °C, with the gas ratio of $Ar:C_2H_2 = 10:1$ (200:20 mL/min).

active nickel (0.5 wt % Ni loading was used in the initial catalyst/support). These figures imply a production rate of 4.4 g(C) g^{-1}(Ni) min^{-1}. This high yield suggests that the Ni nanoparticles formed from thermal decomposition of nickel stearate are very active catalysts.

Figure 4 shows a group of TEM images of the freshly synthesized samples from which it can be seen that the CNFs have a tubular morphology, with an inner diameter in the range of 10−50 nm. A higher magnification image (Figure 4b) of a typical fiber wall shows semiordered graphitic fringes orientated at an angle of about 40−50° to the fiber axis, a structure that is, in overall morphology and dimensions, similar to a herringbone structure.[7,16,17] Despite the defects and dislocations, the

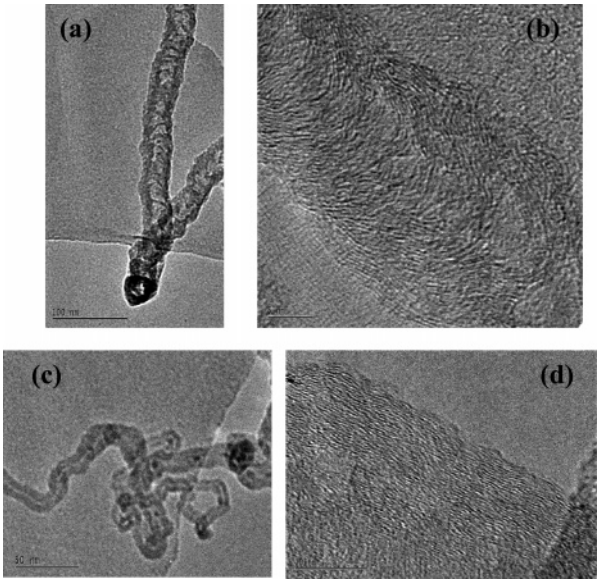

Figure 7. Set of TEM images of the CNFs produced by using either nickel formate or iron acetate catalyst precursor on a sodium chloride support. (a) Typical CNFs produced on the nickel formate/NaCl catalyst. (b) The image at higher magnification shows the herringbone nanostructure. (c) A typical CNF produced on the iron acetate/NaCl powder. (d) A higher magnification image shows the graphitic fringes of a fiber wall.

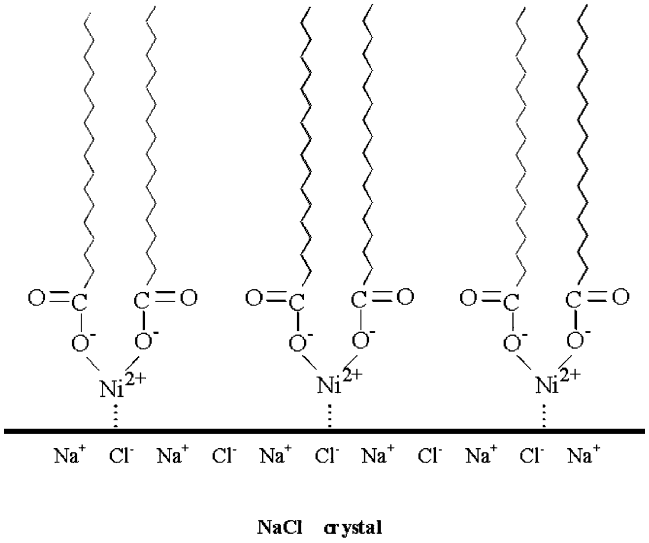

Figure 8. Schematic representation of nickel stearate molecules assembled on the sodium chloride surface. This diagram is a cartoon-like depiction of an ideal case, i.e., the molecular monolayer with the long carbon chains perpendicularly pointing away from the salt surface. In a practical circumstance, there may be several molecular layers on the salt, depending on the surface density of the stearate employed. The carbon chains may also have an angle to the salt surface.

CNFs are, in general, crystalline throughout. The amount of amorphous carbon on the surface is low, which is consistent with the TGA analysis. Metal nanoparticles were frequently found at the end of the CNFs, with a typical pear-drop shape, suggesting a possible tip growth mechanism (Figure 4c). The HRTEM image (Figure 4d) clearly shows that the metal particle is surrounded by crystalline graphitic layers. Laser Raman spectroscopy confirms the graphitic structure (Figure 5), with the characteristic G and D peaks centered at 1601 and 1347 cm^{-1}, respectively. The ratio of these peaks gives the degree of crystallinity within a carbon material. Here, the ratio of G/D $\approx$ 1.1, is reasonable for a CVD-grown nanofiber material.

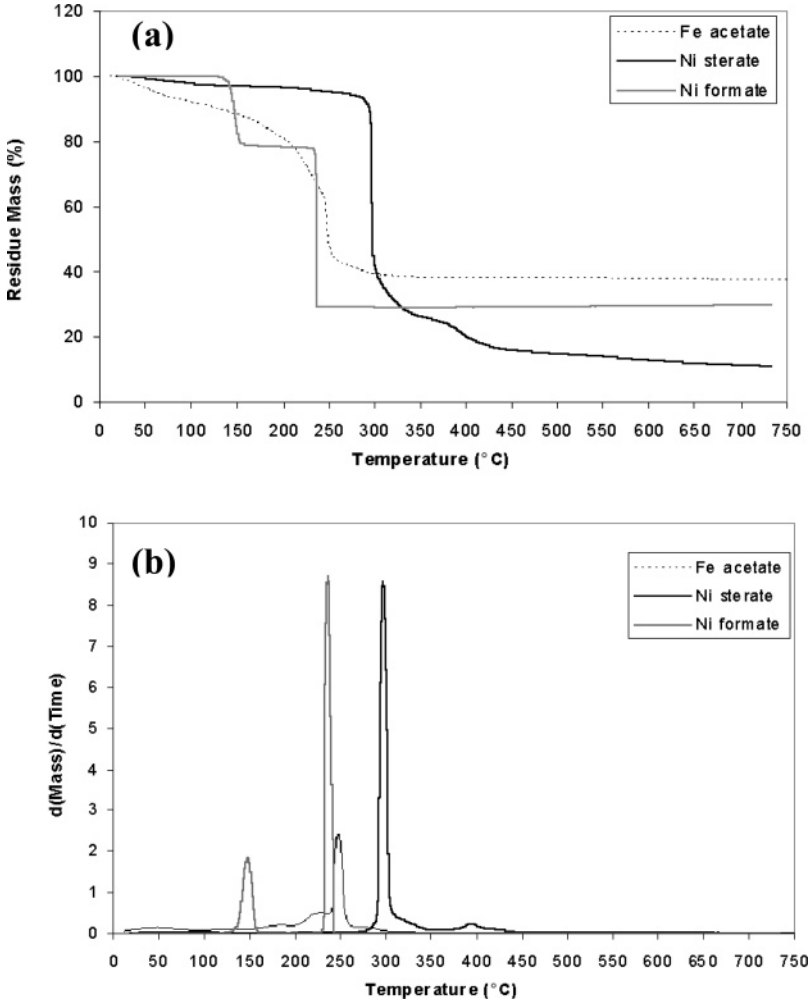

Figure 9. TGA analysis of the thermal decomposition pathways of the three catalyst precursors: nickel stearate, nickel formate and iron acetate. Samples were heated in a N_2 atmosphere, 10 °C/min. (a) Mass-loss profiles as a function of temperature; (b) Differential mass variations against temperature.

3.3. Production of Carbon Nanofibers from the Nickel Formate/NaCl and Iron Acetate/NaCl Catalysts. Figure 6a shows the nanofibers produced from the nickel formate/NaCl catalyst with a 0.16 wt % Ni loading. The fibers have a typical diameter of ∼40 nm, and they are relatively abundant given the low catalyst loading used. They are, however, more curved than those produced by the stearate catalyst, and the coverage of the fibers was less even on the substrate. TEM analysis (Figure 7, parts a and b) found that the fibers posed a typical herringbone structure, which made them have a large number of graphitic edges on their surface. The fibers produced from the iron acetate/NaCl catalyst were of similar diameter (20−60 nm, Figure 6b) but with a different carbon structure; these fibers resembled poorly-crystallized multiwall carbon nanotubes (Figure 7, parts c and d).

TGA analysis (Figure 3) showed the weight-loss occurred at ∼450 and ∼430 °C for the CNFs grown from the nickel formate and iron acetate catalyst, respectively. The result again suggests a low amorphous carbon content, in agreement with the TEM observation. The carbon yields are 7.7 and 2.3 wt %, respectively, relative to the total mass of the support and catalyst. These yields can be converted into the yields relative to the mass of pure catalytic metals, giving 5241 and 7919 wt %, respectively, for the nickel formate and iron acetate catalyst. The laser Raman spectroscopic measurements on both types of CNFs showed the characteristic graphitic G and D peaks (Figure 5), with the ratio of G/D ≈ 0.5 and 1.1, respectively.

3.4. Interaction of the Catalyst Precursors with the Sodium Chloride Surface. The nickel stearate readily forms a highly uniform film on the surface of the sodium chloride powder. No crystalline nickel stearate grains were visible either to the naked eye or under an electron microscope. The uniformity of the deposition may be attributed to the following chemical processes: since NaCl is composed of opposite ions, Na^+ and Cl^-, the surface of the salt crystals is both polar and hydrophilic. On the other hand, nickel stearate is amphiphilic. The polar part is the ionic $(COO)_2^-Ni^{2+}$ group, while the nonpolar contribution is provided by the long carbon chain $CH_3(CH_2)_{16}$. This surfactant structure allows the stearate molecules to organize themselves onto the polar NaCl crystal surface, as the nonpolar solvent evaporates. A schematic representation of the contact interface between the stearate molecules and the NaCl surface is shown in Figure 8. It was observed that the stearate-coated NaCl powder becomes hydrophobic due to the continuous film coverage on the salt surface. In contrast, nickel formate or iron acetate did not form uniform films on the salt support. Instead, upon evaporation of solvent, they formed small crystalline grains distributed over the whole support surface.

3.5. Chemistry of the Thermal Decomposition of the Catalyst Precursors. TGA analyses for the thermal decomposition of all of the three precursors in N_2 atmosphere are presented in Figure 9. Nickel formate first dehydrates at ∼140 °C, and then decomposes at 230 °C into gaseous species

and metallic nickel. Dehydration of iron acetate was followed by its decomposition at 250 °C, although the two processes do not have a clear boundary. The nickel stearate did not have crystalline water in its lattice structure. It was thermally stable until a temperature of ~ 300 °C at which it decomposed.

Nickel formate decomposes directly into metallic Ni nanoparticles without forming the oxide (NiO) intermediate in a gas flow system.[11] This is clearly reflected in the shape of the TGA profile, and the residue mass also well matches the calculated Ni content in the formate (31.6 wt %, in $(HCOO)_2Ni{\cdot}2H_2O$). In comparison, the decomposition of nickel stearate has a rapid start but proceeds slowly at the later stage and thus displays a long tail. There is a middle step in the temperature range of 300−400 °C, presumably caused by formation of an intermediate substance. The whole process has finally finished at a temperature of ~650 °C, where the measured residue mass is close to that of the Ni content in the stearate (calculated: 9.4 wt %). The chemical decomposition process of nickel stearate may be described below

$$n\mathrm{Ni}(\mathrm{CH_3(CH_2)_{16}COO})_2 \xrightarrow{300-600\ ^\circ\mathrm{C}} n\mathrm{Ni} + \text{gases species } (\mathrm{H_2},\ \mathrm{CO},\ \mathrm{CO_2},\ \mathrm{H_2O})$$

In our previous studies, we reported that nickel formate is a useful catalyst precursor in the growth of both single-wall and multiwall carbon nanotubes.[9,11] Comparison of the molecular structures of nickel stearate and formate reveals that both are in general similar, with the only difference being the length of the carbon chain (1 C for the formate, 18 C for the stearate). Bearing this in mind, we speculate that the carbon atoms in the molecules may have played an important role in the cause of the differences of their decomposition pathways. This may partly relate to the different morphologies of the precursors on the support, which may in turn affect the geometry of the metal nanoparticles formed and the morphologies of the carbon nanofibers grown. Further experimental evidence is required for future studies to deduce the exact mechanism involved in the relationships between the decomposition pathways, size and geometry of the metal nanoparticles and the observed differences in morphology of the grown nanofibers. Moreover, pyrolysis of both compounds normally ends up with pure-phase metallic nickel.[11,18] Also, decomposition of both nickel salts is driven by self-redox reactions, in which a nickel atom obtains two electrons from the two carboxyl ligands to be reduced into metallic nickel.

4. Conclusions

We have demonstrated that carbon nanofibers may be grown in high yields on a sodium chloride support. A particular advantage of our method is that since NaCl is water-soluble, separation of the carbon nanofiber product from the support can be easily implemented after the growth. In particular, nickel stearate has been found to be an efficient catalytic precursor for coating the NaCl support. The success of the catalytic system is attributed to the uniform distribution of nickel stearate on the support, which is believed to arise from a surfactant process driven by polar interactions. Furthermore, the self-redox mechanism of thermal decomposition, coupled with the relatively low decomposition temperature, distinguishes nickel stearate from many other inorganic nickel-containing salts, and provides an ideal catalyst/support system for the carbon nanofiber growth.

Acknowledgment. We thank helpful discussions given by Stephen Cash (Thomas Swan Co. & Ltd. U.K.) on this work. J.G., I.K., and C.S. are grateful to Thomas Swan Co. & Ltd. U.K. for financial support.

References and Notes

(1) Baughman, R., H.; Zakhidov A. A.; De Heer, W. A. *Science* **2002**, *297*, 787.
(2) Dresselhaus, M. S.; Dresselhaus, G.; Eklund, P. C. *Science of Fullerenes and Carbon Nanotubes*; Academic Press: San Diego, CA, 1996.
(3) Helveg, S.; Lopez-Cartes, C.; Sehested, J.; Hansen, P. L.; Clausen, B. S.; Rostrup-Nielsen, J. R.; Abild-Pedersen, F.; Norskov, J. K. *Nature* **2004**, *427*, 426.
(4) Endo, M. *Chemtech* **1988**, *18*, 568.
(5) Baker, R. T. K. *Carbon* **1989**, *27*, 315.
(6) Li, Y.; Kim, W.; Zhang, Y.; Rolandi, M.; Wang, D.; Dai, H. *J. Phys. Chem. B* **2001**, *105*, 11424.
(7) Singh, C.; Quested, T.; Boothroyd, C. B.; Thomas, P.; Kinloch, I. A.; Abou-Kandil, A. I.; Windle, A. H. *J. Phys. Chem. B* **2002**, *106*, 10915.
(8) Hata, K.; Futaba, D. N.; Mizuno, K.; Namai, T.; Yumura, M.; Iijima, S. *Science* **2004**, *306*, 1362.
(9) Geng, J.; Singh, C.; Shephard, D. S.; Shaffer, M. S. P.; Johnson, B. F. G.; Windle, A. H. *Chem. Commun*. **2002**, 2666.
(10) Su, M.; Zheng, B.; Liu, J. *Chem. Phys. Lett*. **2000**, *322*, 321.
(11) Geng, J.; Li, H.; Golovko, V. B.; Shephard, D. S., Jefferson, D. A.; Johnson, B. F. G.; Hofmann, S.; Kleinsorge, B.; Robertson, J.; Ducati, C. *J. Phys. Chem. B* **2004**, *108*, 18446.
(12) Li, Y.; Kinloch, I. A.; Shaffer, M. S. P.; Singh, C.; Geng, J.; Johnson, B. F. G.; Windle, A. H. *Mater. Chem*. **2004**, *16*, 5637.
(13) Szabo, A.; Mehn, D.; Konya, Z.; Fonseca A.; Nagy, J. B. *PhysChemComm* **2003**, *6* (10), 40.
(14) Liu, B, H.; Ding, J.; Zhong, Z. Y.; Dong, Z. L.; White, T.; Lin, J. Y. *Chem. Phys. Lett*. **2002**, *358*, 96.
(15) Harris, P. J. F. *Carbon Nanotubes and Related Structures—new materials for the twenty-first century*; Cambridge University Press: Cambridge, U.K., 1999.
(16) Bessel, C. A.; Laubernds, K.; Rodriguez, N. M.; Baker, R. T. K. *J. Phys. Chem. B* **2001**, *105*, 1115.
(17) Boellard, E.; de Bokx, P. K. *J. Catal.* **1985**, *96*, 481.
(18) Geng, J.; Jefferson, D. A.; Johnson, B. F. G. *J. Mater. Chem*. **2005**, *15*, 844.